drones

MDPI

Article

Improving Racing Drones Flight Analysis: A Data-Driven Approach Using Motion Capture Systems

Jose M. Castiblanco Quintero [1], Sergio Garcia-Nieto [2,*], Raul Simarro [2] and Dmitry I. Ignatyev [1]

[1] Centre for Autonomous and Cyberphysical Systems, Cranfield University, College Road, Cranfield MK43 0AL, Bedfordshire, UK; jose.m.c.quintero@cranfield.ac.uk (J.M.C.Q.); d.ignatyev@cranfield.ac.uk (D.I.I.)
[2] Instituto de Automática e Informática Industrial, Universitat Politècnica de València, Camino de Vera s/n, 46022 Valencia, Spain; rausifer@upvnet.upv.es
* Correspondence: sgnieto@isa.upv.es

Abstract: The publication of the previous study, titled "Experimental Study on the Dynamic Behaviour of Drones Designed for Racing Competitions", highlighted the increasing interest in employing scientific methods for their design and analysis. That study examined the flight data of 15 racing drones within a large flight area, using Doppler-type sensors for data collection. Building on these findings and seeking to enhance them, the current work introduces an upgraded data acquisition system utilising optical sensors, thereby improving measurement accuracy. These enhanced flight data facilitate the development of updated quality indices and conclusions, offering a more precise and definitive analysis than was previously possible.

Keywords: drone; airframe; high performance; structure design; data analysis; agile; flight dynamics

Citation: Castiblanco Quintero, J.M.; Garcia-Nieto, S.; Simarro, R.; Ignatyev, D.I. Improving Racing Drones Flight Analysis: A Data-Driven Approach Using Motion Capture Systems. *Drones* **2024**, *8*, 742. https://doi.org/10.3390/drones8120742

Academic Editor: Yushu Yu

Received: 5 November 2024
Revised: 28 November 2024
Accepted: 1 December 2024
Published: 9 December 2024

1. Introduction

This paper seeks to update and enhance the flight data measurements presented in the previously published study, "Experimental study of the dynamic behaviour of drones designed for racing competitions", by employing a high-precision optical motion system (OMS). As demonstrated in [1] and various other research contexts [2–4], racing drones are having an exponential impact on the emerging e-sports sector. Consequently, introducing improvements to any of their components is of significant importance. In particular, studying and analysing the behaviour of different airframe geometries is critical in enhancing the dynamic performance of racing drones. For this reason, in the earlier study [1], Doppler-type sensors with medium-to-low accuracy were used to acquire flight data for the analysis. This updated study implemented a higher-precision OMS to obtain more meaningful and accurate flight datasets, enabling an updated and improved analysis.

The previous study addressed these issues using traditional methods. It facilitated flight tests conducted through case studies on a standardised race track [1]. The body shapes of the racing drones were normalised with the distance between the motors defined as the lambda (λ) distance. The angles between the arms were standardised as the alpha (α) and beta (β) angles. Consequently, the following airframe configurations were identified: symmetrical, non-symmetrical, and hybrid. The pilots' expertise also played a crucial role in the earlier study, as they guided the motion of the drones in terms of agility, manoeuvrability, and stability. Furthermore, they categorised various race tracks, such as wide, compact, tracks with numerous obstacles, or high-speed tracks.

Previous testing studies considered a classic or standardised racetrack [1], which is characterised by track areas with long and wide sections. In contrast, this study focuses on a racetrack with smaller and narrower sections. Additionally, to address earlier reviews, this study utilised a database specialised in racing drones [5], which served as the primary foundation for our current analyses. Furthermore, we employed an OMS to capture

the drones' motion, replacing the Doppler sensor system used in the previous study. Specifically, we analysed the motion of 15 airframe models, and the results were compared against the expertise of skilled pilots. Other studies have utilised simulation platforms [6] to investigate the flight dynamics of racing drones. These platforms enabled the management of model trajectories and guidance by creating a 3D racetrack defined by waypoints. Consequently, the motion of the models was analysed through the thrust effort exerted by the voltage regulators.

In this new study, we update and provide a more detailed analysis of the dynamics of racing drones. Building on previous findings, we enhance the quality of the results and aim to complement and expand the scope of the earlier research. Furthermore, we conducted a comparative study and established correlations between airframe geometries and the newly observed trajectories.

Table 1 highlights the exceptional capabilities of the OMS in demanding applications [7]. Its superior data accuracy enables precise tracking with millimetre-level precision and robust reconstruction algorithms, making it highly suitable for scenarios such as racing drone tracking. The system's real-time capabilities are also noteworthy, offering sub-10-millisecond latency and practical frame rates of up to 900 Hz [8]. This critical feature provides confidence in its performance within fast-paced environments, such as robotic assembly lines. Moreover, the OMS's adaptability in high-complexity scenarios, including maintaining performance in environments with dense or occluded markers, underscores its reliability, as demonstrated in drone swarm tracking. Finally, the system's advanced synchronisation capabilities make it a dependable tool for integrating motion capture with other devices, as demonstrated by its success in biomechanical analyses and complex systems like simulation platforms [6].

Table 1. Some capabilities and demanding applications for the optical motion system—OMS.

Measurable Aspect	Specific Details
Data accuracy	Metrics/Capabilities: - Centroid detection: 10-bit greyscale data (brightness levels: 0–1023). - Marker separation: Adjustable from 0 to 100.0 mm. - Reconstruction accuracy: At least three cameras; supports up to 50. - To virtually track up to two cameras. - Drift tolerance: Configurable in millimetres for calibration stability. Case study: - Racing drone tracking: Tracking drones at 80.0–150.0 km/h with five cameras, achieving 0.3 mm marker accuracy and <10.0 ms latency, even with challenges like reflections and abrupt manoeuvres. As a reference, example [1,9].
Real-time capabilities	Metrics/Capabilities: - Low latency: Under 10 ms with real-time buffer size configurable from 1 to 100 frames. - Frame rates: Cranfield University-Flight Arena cams up to 240 Hz. - UDP streaming: Data packet sizes of 256, 512, or 1024 bytes. Case study: - Collaborative robotics: In a robot assembly line, with a 500 Hz capture rate, ensuring real-time adjustments and collision prevention among robots in a dynamic environment. As a reference, example [10].
High-difficulty scenarios	Metrics/Capabilities: - High marker density: Differentiates markers by circularity and blob height. - Adaptable drift tolerance for small and large volumes. - Robust reconstruction: Uses jitter reduction algorithms for clarity. Case study: - Drone swarm tracking: Monitoring 20 drones with five markers each in a 20 m^3 volume using 15 cameras. Achieved real-time tracking with <20 ms latency, handling occlusions and overlapping flight paths effectively. As a reference example [11].

Table 1. *Cont.*

Measurable Aspect	Specific Details
Complex synchronization	Metrics/Capabilities: - Genlock and Timecode: Supports external synchronization for seamless multi-device setups. - Flexibility: Synchronizes at standard frame rates (e.g., 240 Hz). Case study: - Biomechanics analysis: Synchronized optical motion capture with force plates and EMG sensors at 240 Hz ensures precise muscle activity correlation with motion for diagnosing movement disorders. As a reference example [12].

An OMS has been adopted to track dynamic behaviour. Vicon Tracker software precisely captures motion by tracking objects using a centralised network of cameras. Unlike Vicon Shogun, which is commonly used in the entertainment industry to track people, Vicon Tracker offers superior accuracy and rapid feedback for locating moving objects. Table 2 highlights the system's main features. It provides real-time processing with minimal latency and supports offline storage to manage large volumes of data. Furthermore, it accommodates sampling rates of up to 240 Hz, enabling more detailed and flexible post-analysis. Additionally, the software facilitates data transfer between dissimilar applications and supports multiple communication protocols. It can even track motion with a single camera, minimising interruptions in data capture. Its high capture speed makes it particularly well suited for dynamic applications such as drone tracking [8].

Table 2. Technical features of Vicon Tracker software.

Feature	Description
User-friendly interface	Simplifies calibration and workflows, allowing users to focus on essential tasks without unnecessary complexity.
Real-time processing	Provides latency as low as 1.5 ms and supports capture speeds exceeding 500 frames per second, ideal for applications requiring immediate responsiveness.
Simulink integration	Enables communication via UDP for hardware-in-the-loop (HIL) testing and real-time feedback in robotic systems.
Multi-protocol compatibility	Supports UDP, TCP, VRPN, and Vicon DataStream SDK, enabling seamless integration with Windows, Linux, and .NET platforms.
Single-camera tracking	Maintains object tracking even when markers are visible to only one camera, minimising disruptions.
High-speed tracking	Tracks multiple objects at high speed, essential for dynamic systems such as agile robotics.
Large-volume capture	Utilises active markers for accurate tracking in expansive spaces, such as warehouses or test areas.
Automatic system calibration	Continuously monitors and adjusts calibration, reducing the need for manual intervention.
High sampling rates	Supports rates of up to 240 Hz, ensuring accuracy in capturing fast movements.
Offline data storage	Allows flexible post-processing and detailed analysis of recorded data.

It utilises luminescent trackers on the drone airframe [13,14] to effectively capture the drone's motion [15,16]. The system includes a network of cameras that records the drone's position in real time [17,18]. These systems are particularly advantageous in GPS-denied environments because they provide highly accurate recorded data [19,20], which is a defining feature. Consequently, machine learning algorithms often use these data for drone training [3,21,22]. However, a key limitation lies in the flight testing areas, which are often confined compared to traditional racing tracks. See Table 3.

Table 3. Flight testing areas.

Race Tracks	Length	Width	Height	System	Sensor
Cranfield University	20.0 m	20.0 m	4.0 m	OMS—Vicon	30 cameras
University of Zurich	30.0 m	15.0 m	6.0 m	OMS—Vicon	50 cameras
Traditional racing track	60.0 m	45.0 m	20.0 m	Doppler effect	8 devices

The system encounters technical challenges that can impact the accuracy and quality of the data. One of the most common issues is camera occlusion, where markers move out of the field of view due to subject motion, obstacles, or improper camera placement [23,24]. To address this, the strategic placement of additional cameras and markers within the volume is commonly employed, as outlined in Table 4. Following ISO 10360-10:2021 standard is typically encouraged to ensure dimensional accuracy in optical systems. Additional challenges include reduced marker visibility and insufficient technical training, leading to calibration errors outside standard specifications. Among these, the most frequent issue is cold cameras, which compromise the consistency of the captured data.

Given the experimental setup of the study and the nature of the sensors, it is essential to examine potential sources of error and their impact on measurement (see Table 5). This approach links the limitations and scope of the analysis [7,25].

Table 4. Technical issues and related International Organization for Standardization (ISO) standards.

Typical Issues	Description and ISO Standards
Camera occlusion	- Markers may exit the camera's field of view due to motion, obstacles, or suboptimal camera placement. - Solution: Strategic camera placement and the use of additional markers. - The ISO standard in [26] concerns ensuring dimensional accuracy in optical systems.
Insufficient lighting	- Poor lighting conditions reduce marker visibility and affect tracking quality. - Solution: Infrared lighting and adjustments to camera sensitivity. - The ISO standard [27] specifies minimum lighting requirements.
Marker placement	- Incorrect marker positioning leads to errors in motion reconstruction. - Solution: Place markers at key anatomical or structural points and ensure personnel are adequately trained. - The ISO standard [28] provides guidance for precise marker placement.
Calibration errors	- Inaccurate calibrations result in data inconsistencies. - Solution: Use robust calibration procedures, ensure cameras are pre-warmed, and verify results. - The ISO standard [29] ensures reliable calibration standards.
Quality standards	- Maintaining overall system quality is essential for reliable and consistent data. - Solution: Regular inspections and documented protocols. - The ISO standard [30] establishes frameworks for high-quality processes.

In particular, marker duplication presents a significant challenge in high-speed drone racing during tight turns. This issue occurs when reflective surfaces or overlapping trajectories produce false signals, compromising tracking accuracy. Additionally, corners of the volume may become black or blind spots due to camera placement, resulting in unmeasurable areas. A state-of-the-art lighting system and an L-shaped sensed volume restriction aim to mitigate these issues by minimising reflective artefacts and improving marker resolution using high-intensity synchronised strobe lights. This spatial configuration, combined with the Vicon camera layout, enhances marker detection even during tight turns. Technically, it reduces noise by improving centroid adjustment.

These advancements enable accurate trajectory reconstruction, establishing Cranfield's flight arena as a reference for studying drone performance and flight dynamics in complex and demanding environments.

Table 5. Sources of error in OMS measurement and mitigation actions.

Source of Error	Practical Considerations for Mitigation
Environmental lighting	- Impact: Ambient light interference can create false markers or reduce tracking accuracy. - Quantification: Threshold adjustable from 0 to 1; low jitter mode is effective but bandwidth-sensitive. - Mitigation strategies: Adjust the threshold; use low litter mode; minimise reflective surfaces.
Camera occlusion	- Impact: Occlusion blocks the line of sight, leading to incomplete trajectory reconstruction. - Quantification: Minimum cameras required: 3; increasing to 4 or 5 reduces occlusion errors. - Mitigation strategies: Increase the minimum number of cameras to 4 or 5; optimise camera placement.
Sensor inaccuracy	- Impact: Calibration drift due to environmental factors causes inaccuracies. - Quantification: Drift tolerance adjustable to 2–5 mm; calibration achieves <0.5 mm accuracy in a 5 × 5 × 3 m volume. - Mitigation strategies: Perform routine calibration; adjust drift tolerance based on environmental conditions.
Combined effects	- Impact: Combined issues significantly increase reconstruction errors. - Quantification: Trajectory errors increased from 0.2 mm to 0.7 mm; recalibration reduced this to 0.3 mm. - Mitigation strategies: Perform regular recalibration and combined adjustments to thresholds and camera configurations.

This study remains focused on experimentation. This time, tests are conducted on sectors with short trajectory lines and tight turns. Consequently, the performance indicators are aligned with the motion within these sectors of the race tracks. Due to its straightforward layout, the TRAMP FPV Racing database is utilised as a statistical analysis tool, allowing the accuracy of the stored data to be fully exploited. The new dataset, significantly larger than the previous one, improves the quality of the results. Attention is drawn to an overview of earlier findings, which are revisited in Section 2.

As the new results emphasise extensive data analysis, a brief report on the OMS used to create the database is presented in Section 3. The methodology is reviewed in Section 4, where the database fits are also verified. Section 5 explores the new results from the OMS, employing the box-and-whisker plot method. Earlier results are compared to the new ones with accelerometer data incorporated to enhance the analysis. Finally, the findings on racing drone performance are summarised and shared.

2. Summary of Previous Findings

A lack of scientific knowledge regarding the design of race-quality quadrotors was identified [1]. As a result, the performance of 15 airframe models was examined. The expertise of skilled drone pilots was compared (see Table 6) with the records stored by four Doppler sensors (see Table 7). The pilots distinguished the drone's behaviour on the straights and turns of the racing track.

The essentials of the data recording process are presented in Table 7. It should be noted that the experiments were conducted on a large indoor racetrack. The Doppler sensors were also positioned at four precise points along the track. A total of 1000 samples were collected for each model tested. Behavioural indices (J) were used to categorise the sample data within specific sectors of the track based on the placement of the sensors. Subsequently, box-and-whisker plots were employed to analyse the datasets. Each model was assigned an index for straight-line speed (J1), turn sector speeds (J2), and realised turn time recorded during curved trajectories (J3).

Table 6. Flight sensations.

Total Pilots Interviewed 55	SY	NSY	HS
Stability 20/36.3%	13 65.0%	5 25.0%	2 10.0%
Agility 30/54.5%	4 13.3%	25 83.3%	1 3.3%
Manoeuverability 13/23.6%	9 69.2%	4 30.7%	0 NN%
Overall size 23/41.8%	8 34.8%	12 52.1%	3 13.0%
Control setting 15/27.2%	1 6.6%	7 46.6%	7 46.6%

Table 7. Characteristics of previous flight tests.

Racing Track Description	Description of the Test Flight	General Features
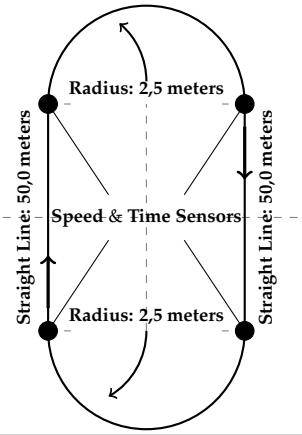	Details: - Type of race track - Straight sectors - Straight line length - Radius of the curves - Number of drones - Number of sensors - Number of test pilots - Number of laps - Number of repetitions - Samples registered	Values: - Left hand—Indoor - Two (2) - 50 m - Two (2) - Fifteen (15) - Four (4) - One (1) - Four (4) - Ten (10) - Thousand (1000)

2.1. Expertise Shared by the Pilots

Table 6 presents the expertise of the trained pilots, organised in percentage form and based on the most frequently used terms. Notably, the highest percentages are associated with the symmetric geometric models (SY), except for agility, where the non-symmetric models (NSY) score higher. Hybrid models (HS) show the lowest percentages across all queries.

The pilots' statements are summarised as follows: pilots identified three basic geometric structures of racing drones: symmetric (SY), non-symmetric (NSY), and hybrid (HS) airframes. They noted that SY airframes exhibit high manoeuvrability in straight-line motion. However, NSY airframes are preferred for their superior performance in tight turns. Additionally, NSY models demonstrate greater agility in turn sectors than any other airframe, making them the most commonly chosen geometric structure. Based on these initial observations, the airframes were classified according to their geometric characteristics, as shown in Table 8. Manoeuvrability and agility were also defined accordingly.

Table 8. Wheelbase: $200.0 \leq \lambda \leq 250.0$ mm.

Basic Airframe	Geometry Description	Geometrical Features
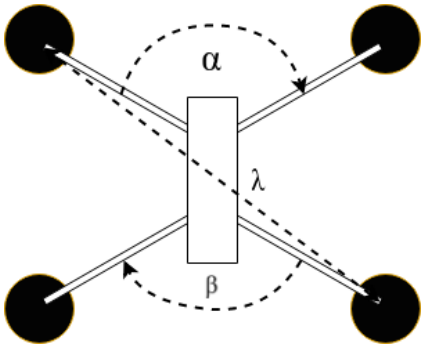	Key characteristics: - Symmetric (SY) - Non-symmetric (NSY) - Hybrid (HS) - Aspect ratio (AR) - Overall size (width × length)	Geometric definitions: - $(\alpha, \beta) \equiv 90.0^{\circ}$ - $65.0^{\circ} \leq (\alpha, \beta) < 90.0^{\circ}$ - $\alpha \equiv 90.0^{\circ}, \beta \neq 90.0^{\circ}$ - $legs(\alpha$ and $\beta)/\lambda$ - Side-by-width relationships

First, the number of times the highest speed is repeated in long, straight sectors is considered. Second, the number of times the highest speed is repeated in tight turns is analysed. Both factors take into account lap times and acceleration profiles. This way, the behavioural indicators (J1 and J2) were linked to these descriptions. The main findings are summarised below. Additionally, SY, NSY, and HS are identified as the most standard airframes. Nevertheless, vertically non-symmetrical and cross-shaped designs were also observed. It should be noted that the wheelbase ranges between 200 and 250 mm. Table 9 summarises the performance of the models, highlighting that designs with angles greater than 75 degrees exhibit outstanding performance when combined with lambda lengths of less than 210 mm. This is largely consistent with pilot statement number two.

The J2 indicator revealed that SY models perform better in tight turns due to their lower top speed. However, this contradicts pilot statement number three. It can be concluded that the geometric design of SY models enhances motion stability.

Table 9. Quantitative summary: racing drone performance.

Characteristic	J1—Manoeuvrability	J2—Agility	Top Speed
λ (mm)	<210.0	<210.0	<200.0
α, β (Degrees)	$75.0^{\circ} \leq (\alpha, \beta) < 90.0^{\circ}$	$(\alpha, \beta) \equiv 90.0^{\circ}$	$80.0^{\circ} \leq (\alpha, \beta) < 90.0^{\circ}$
AR	$0.375 \leq AR \leq 0.39$	$0.204 \leq AR \leq 0.225$	$0.20 \leq AR \leq 0.2225$
wXl (mm^2)	148.492	155.563	147.454×128.557
Weight (g)	$282.58 \leq g \leq 331.86$	$266.90 \leq g \leq 311.14$	$278.77 \leq g \leq 281.58$

Table 10 categorises performance into high, medium, and low levels. NSY models demonstrated moderately high performance. To translate this into a design advantage, angles exceeding 80 degrees are necessary. Additionally, shorter wheelbases of 210 mm are required. Control actions are recommended to adapt the airframe torque accordingly.

Table 10. Qualitative summary of racing drone performance.

Airframes	J1—Manoeuvrability	J2—Agility	Top Speed
SY	Medium	Low	Low
NSY	High	Medium	High
HS	Low	High	Medium

2.2. Brief Outline of the Dynamic Behaviour Profiled

Figures 1 and 2 summarise the behaviours based on speed data repeatability and model weights. It is worth noting that HS models with wheelbases shorter than 220 mm remain an intermediate choice. Nevertheless, NSY models exhibit the narrowest range of

wheelbase options. In contrast, SY models span nearly the entire wheelbase range, covering most configurations while leaving only a few minor alternatives. All wheelbase designs must ensure angles greater than 75 degrees for outstanding performance.

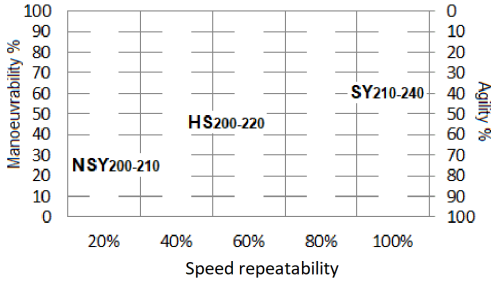

Figure 1. Overview: dynamic behaviour as a function of speed.

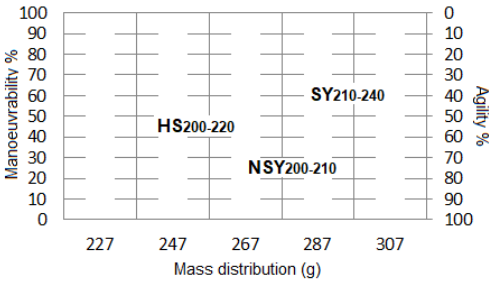

Figure 2. Overview: dynamic behaviour as a function of weight.

NSY airframes feature α and β angles that differ from 90 degrees, allowing them to form horizontally or vertically extended structures. Theoretically, this geometric characteristic provides greater momentum during tight turns. To harness this geometric advantage, two considerations must be addressed. Firstly, the arm length or wheelbase must be appropriately configured. Secondly, aligning this feature with the necessary control settings is strongly recommended. Otherwise, the geometric enhancement will not yield the intended effects. It is also not recommended for beginner pilots or trainees.

Data dispersion was employed as a tool to validate the results. Drone performance was qualitatively categorised into high, medium, and low levels. SY models demonstrated high data compactness, unlike NSY models, which exhibited varying behaviour in fast curves. Meanwhile, among other available solutions, HS models were identified as an intermediate or medium design choice.

2.3. Description and Shape Layout for the Racing Drones Tested

This database includes five types of racing drones with the primary distinction being their geometric shape. Accordingly, their dynamic behaviours are influenced by this characteristic [1]. These drones are classified as symmetric (SY) airframes, non-symmetric (NSY), or hybrid (HS).

In the current study, the ranges of angular distances (α) were adjusted to ensure a more representative analysis of the airframe models under race conditions, considering the size limitations of the flight arena. In other words, this approach builds on the representative models used in the previous study. Unlike the earlier experimental study conducted on broader tracks, where the HS airframe exhibited the widest range of 90° to 90° for both (α) and (β), the selected representative models expand the perspective by focusing on ranges that capture operational variations across all airframe types.

Figure 3 illustrates the geometric configurations of the airframes. The SY airframe features 90° angular distances with 210 mm and 250 mm wheelbases. The NSY airframe exhibits angular clearances ranging from 65° to 80° with wheelbases of approximately 210 mm and 230 mm. In contrast, the HS airframe combines angular distances of 80° in the

upper arms and 90° in the lower arms with a wheelbase of 250 mm. As a result, the models highlighted in the previous study are identified as providing the most statistically accurate dynamic behaviour.

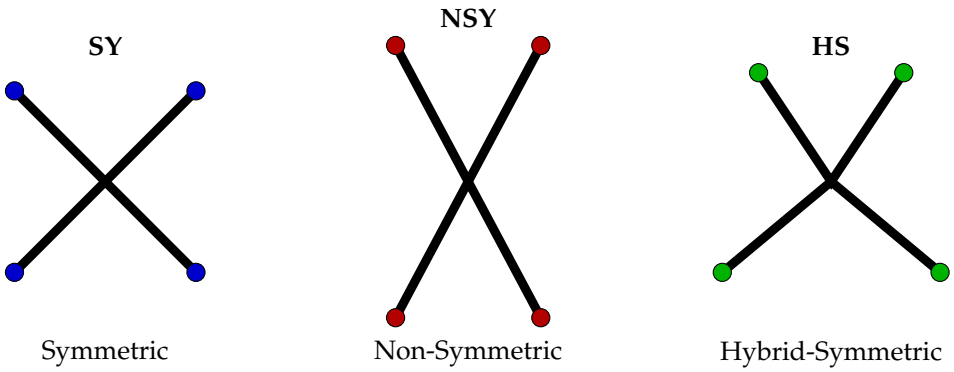

Figure 3. Main geometric topology. Representative airframes for racing drones.

Figures 4–6 illustrate the drones used in the ongoing flight tests. The arm lengths were preprogrammed in the firmware of their specific flight controllers to ensure consistency. Additionally, the radio control levers were set to default values to maintain uniformity across tests. This configuration allows the effect of the airframe shape on the trajectories to be captured in a natural flow. Figure 5 also displays the positioning of the fluorescent grey markers. Each marker is a 14 mm diameter ball covered with fluorescent textiles. They are placed in asymmetrical locations with a 10 mm gap to enable the OMS to reconstruct their positions more efficiently during motion.

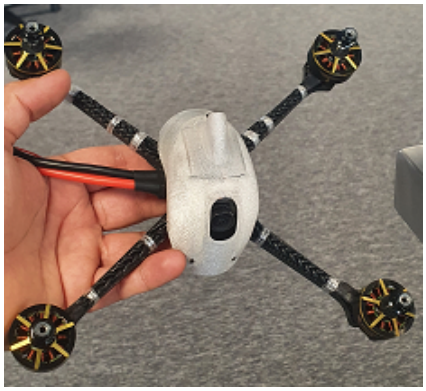

Figure 4. HS shape.

Figure 5. SY shape.

Figure 6. NSY shape.

3. Methodology of Analysis

The analysis methodology consists of three subparts that guide the analytical process. The first subpart addresses the definition of new performance indicators, providing a framework for enhancing and evaluating the dynamic behaviour of racing drones. It examines the impact of specific indicators designed to measure speed, agility, and stability during straight and curved trajectories while accounting for the size constraints of the flight arena. The second subpart focuses on statistical analysis using box-and-whisker plots. It employs descriptive statistical methods to compare and resolve performance variability across airframe models. The final subpart pertains to the setup of the database for statistical analysis. It describes data processing using the TRAM FPV database, emphasising data cleaning, transformation, and organisation. This ensures the reliability and clarity of the statistical outcomes by leveraging robust datasets that accurately capture the drones' dynamic behaviour under controlled conditions. Together, these subparts provide a systematic approach to the analysis, expanding the understanding of the impact of airframe geometry on drone performance. This methodology delivers fresh and robust insights reinforced by quantitative analysis.

3.1. Indicator Framework for Drone Performance

Three performance indicators were proposed in the previous research [1]: J1 for speeds on straight trajectories, J2 for speeds during overturns, and J3 for turn times, as previously defined. These indicators were designed to store data from classic long racetracks. However, new indicators are introduced for confined spaces: J4 for speeds over short, straight trajectories and J5 for speeds in tight turns. Acceleration data will be represented by indicator J6, which, due to the vast dataset, will serve as a behaviour validator.

3.2. Statistical Insights Through Box-and-Whisker Analysis

The same analytical technique will be applied to observe the behaviour of the indicators (J) using a box-and-whisker diagram. The data will be collated using a MATLAB script and organised by sectors of the flight track. Six diagrams will be created, corresponding to the sectors of straight lines and turns. Each diagram contains five boxes representing the data for each model. The boxes cover three quartiles, while the whiskers represent the minima and maxima of the data. This approach enables the analysis of dispersion, concentration, and the range between quartiles. Finally, the findings will be linked to the previous results.

3.3. Setting Up the Database for Statistic Analysis

The data collected from the sensors have been systematically organised into folders and categorised based on the tested airframe geometries (SY, NSY, and HS). Each category divides the data into individual test sessions (e.g., test1, test2, test3). Each test directory

contains synchronised video recordings in WEBM format and complementary data files in CSV format. The files in the BETA and VICON folders have been compressed, encapsulating critical information about the drones' dynamic behaviour and enabling detailed analysis. The organisation and physical significance of the dataset fields are summarised in Table 11.

The dataset provides a comprehensive and detailed collection of dynamic flight data, enabling robust analysis and characterisation of drone behaviour. The Power Query editor was employed to clean and transform the dataset in preparation for analysis. The entire data array was fully utilised. However, due to exceeding the vertical storage capacity limits of the editor, each transformation was saved as a stand-alone file. These cleaned datasets were subsequently converted into MATLAB scripts, specifying, in particular, the column or index that was analysed.

The MATLAB code processes each of the cleaned Excel sheets. Data are read column by column from all Excel sheets, following the arrangement of the tests performed and the battery consumption ratios. This approach enables the direct extraction of translation signals and angular velocities from the database for each model.

Table 11. Structure and physical significance of dataset fields.

File Type	Field	Physical Description	Relevance Information
IMU CSV Files	Roll, Pitch, Yaw (deg/s)	Describes the rotational motions involved in turning the drone.	Enables attitude dynamic analysis.
	X, Y, and Z—Axes Acceleration	Linear motion behaviour in raw units (2048 units = 1 g).	The sensor measures ranges from $\pm$2 g to $\pm$16 g.
	Heading Angles	Orientation angles relative to the initial position.	Supports local drone location and system calibration.
OMS CSV Files	Frames per Second (fps)	Sampling rate to create the motion effect.	Ensures temporal precision for data synchronisation.
	Rotational Data (RX, RY, RZ)	Enables angular rates to be analysed.	Expressed in radians for 3D motion reconstruction.
	Translational Data (TX, TY, TZ)	Position in millimetres along the X, Y, and Z axes.	Validates trajectories and assesses displacement.

The signals are computed via numerical derivation at a sampling rate of 0.001 s. Subsequently, the signal is segmented by sectors and their respective lengths. Finally, the signal is indexed to extract the relevant data for further statistical analysis. Notably, all columns have been labelled with their respective indices and manually marked as J4, J5, and J6. Additionally, the intervals between direction changes have been automatically labelled as curved (S2) or straight sectors (S1) and manually cross-checked. This ensures efficient processing and integration for advanced statistical analysis.

This approach facilitates a precise and in-depth representation of drone dynamics, aligning with the statistical methods introduced in this study. Furthermore, the dataset structure and transformation process establishes a foundation for training machine learning algorithms focused on navigation, contributing to developing robust, data-driven methodologies in aerial robotics research.

3.4. Essential Insights About the Database

The TRAM FPV database will be utilised to study the behaviour of racing drones [5]. It is hosted at Cranfield University, England. Its features are as follows: the CSV-IMU files contain 11 columns with approximately 90,000 rows, which are organised as shown in Table 12.

Table 12. Dataset—IMU.

Row	Description	Magnitude	Error (%)
1	loopIteration	<1,284,656.0	0.0
2	Local Time	µs	0.0
3	Roll axis rotation	deg/s	<0.01
4	Pitch axis rotation	deg/s	<0.01
5	Yaw axis rotation	deg/s	<0.01
6	X-axis acceleration	raw	<0.1
7	Y-axis acceleration	raw	<0.1
8	Z-axis acceleration	raw	<0.1
9	Roll heading	raw	<0.09
10	Pitch heading	raw	<0.09
11	Yaw heading	raw	<0.09

This table presents three rotations, accelerations, and heading angles relative to the coordinate axes (X, Y, Z). Additionally, the data are smoothed using a low-pass filter. The CSV-Vicon files contain 8 columns with approximately 50,000 rows, which are organised as shown in Table 13. This table includes three rotations, translations, and the sample rate in frames per second. It is important to note that the rotation order follows a helical sequence. Specifically, the rotation is relative to the position of the marker at various time instants, allowing it to be transformed into non-instantaneous rotation. The most common representations are Euler or quaternion angles. The errors are expressed as rate coefficients provided by the tracker software.

Table 13. Dataset OMS-Vicon.

Row	Description	Magnitude	Error (%)
1	Frames	fps	<0.017
2	Subframes	0.0	NA
3	RX X-axis rotation	rad	0.397–0.79
4	RY Y-axis rotation	rad	0.397–0.79
5	RZ Z-axis rotation	rad	0.397–0.79
6	TX X-axis translation	mm	<0.149
7	TY Y-axis translation	mm	<0.149
8	TZ Z-axis translation	mm	<0.149

Table 14 describes the tools used to construct the database. The behaviour of two symmetric models (SY), two non-symmetric models (NSY), and one hybrid model (HS) will be analysed. Additionally, row 6 of the OMS data and row 7 of the IMU data will be utilised, corresponding to the translation and acceleration data.

Table 14. Database summary.

Database	Description	Features
Kind of airframes	SY, NSY, HS	$210.0 \leq \lambda \leq 250.0$ mm
Numbers of drones	5 airframe models	$65.0^\circ \leq (\alpha, \beta) \leq 90.0^\circ$
Indoor sensors	IMU/OMS	30 cameras—Vicon
IMU data	Y-axis acceleration	500 Hz
OMS data	TY Y-axis translation	240 Hz
Flight sequences	150 sequences	30 sequences per drone
Flight arena	20 × 20 m	Cranfield University

The electronic layout of the models is outlined in Table 15. These models are specifically designed for racing drones and were all supplied by the same manufacturer. Additionally, the PID controller settings are configured to their default values.

Table 15. Setup of the models.

Electronic Components	Specifications
Flight controller	F7—Tmotor
ESC	55 mA—Tmotor
Video transmitter	VTX Viva FPV—Tbs
Radio receiver	R-XSR—FrSKY
Antennas	Linear Emax
Battery	6 s–4 s
Propellers	5147—Tmotor
Motors—Tmotor	F60PRO 1950–2550 Kv
Firmware	Betaflight

4. Analysis of the Results

The data provided in the TRAM-FPV database will be utilised for the analyses. This database contains flight sequences in confined spaces and is specifically focused on studying racing drones. Initially, the data extracted from the database will be described, which is followed by a presentation of the models' behaviour. The analyses are divided into four parts, culminating in a comparison to validate the results.

Table 16 details the data used for the analysis. The models have wheelbases ranging from 220 to 250 mm with angles equal to 90 degrees. The weights of the structures range from 292 to 342 g, and the total size varies between 133 and 170 mm. Additionally, the total balance of IMU data exceeds the row limits available in Excel, while the OMS data occupy approximately 75% of the sheet. The IMU data have been trimmed to fit the maximum available capacity.

Table 16. Data analysed by model.

Airframe (mm)	Overall Size (mm^2)	Data IMU/OMS
SY250/$(\alpha, \beta) \equiv 90.0^\circ$	163.0×163.0	1,048,000.0/774,583.0
SY220/$(\alpha, \beta) \equiv 90.0^\circ$	137.0×137.0	738,084.0/533,292.0
NSY220/$70.0^\circ \leq (\alpha, \beta) \leq 90.0^\circ$	133.0×159.0	746,319.0/669,278.0
NSY240/$80.0^\circ \leq (\alpha, \beta) \leq 90.0^\circ$	139.0×180.0	791,067.0/633,791.0
HS250/$\alpha \equiv 80.0^\circ, \beta \neq 90.0^\circ$	134.0×170.0	664,986.0/380,875.0

4.1. General Layout of the Track

Figure 7 illustrates how the data are segmented into sectors. Sector S1 represents speeds on straight lines, while S2 corresponds to speeds on curves. Notably, each sector is associated with a performance index: J4 and J5. Additionally, the acceleration indicator (J6) is included within these sectors.

Figure 7. Racing track sectors.

4.2. Flight Sector 1 (S1)—Performance Indicator: Straight Trajectories (J4)

This section describes the speed behaviour of the models and consists of two figures and two tables. Additionally, a time indicator per sector is included. The figures and tables outline the behaviour of various racing drone models in straight trajectory sectors (S1). The figures visually represent the models' speed distributions and timing performances, capturing variations in their behaviour. One figure highlights the speed probabilities of the models across multiple trials, while the other illustrates the corresponding time indicators for completing straight sections of the track. The tables complement these visual representations by providing numerical data on key performance metrics. One table summarises each drone model's speed quartiles, medians, and maximum values, while the other details the time statistics, including quartiles and ranges. Together, these figures and tables present a concise yet comprehensive overview of the performance trends observed in the airframes tested, aiding the interpretation of their straight-line dynamics. These resources support the organisation of the results for practical analysis. Tables containing the most relevant numerical data from the graphs are expressed differently. Consequently, a set of performance aspects will be established, considering the geometrical features of the models and their performance across the track sectors.

Figure 8 features five racing models. On the left, the first two are non-symmetrical with 220.0 mm and 240.0 mm wheelbases. The last two models are symmetrical with 220.0 mm to 250.0 mm wheelbases. At the centre of the figure is the hybrid model, which has a wheelbase of 250.0 mm. Firstly, it is observed that the data are more compact at lower speeds. The highest speeds deviate from the median line, indicating they are isolated points rather than following a trend. Secondly, the medians of the data warrant attention. Symmetric models exhibit the lowest speeds among the group. In contrast, the speed of the non-symmetric models is notable. Nevertheless, the hybrid model serves as an intermediate alternative. For each model, the magnitudes of speeds and times are described according to the behaviour of the quartiles.

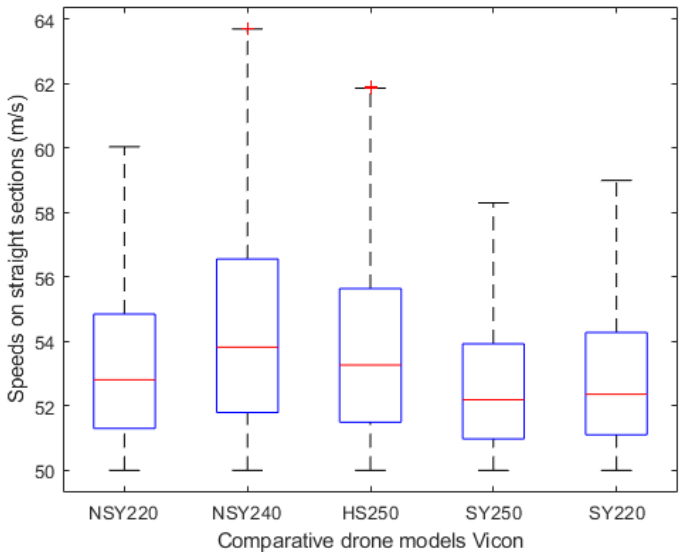

Figure 8. Performance indicator J4.

Table 17 ranks the models from the highest to the lowest speeds. Firstly, it is observed that the lowest speeds remain at 51 m/s in the first quartiles (Q1). Consequently, the average speed differences arise from the final speeds of the third quartile (Q3). The hybrid model is positioned as the second option. In contrast, the NSY240 model achieves 1.6 m/s more than the SY250 model.

Table 17. Speed straight behavior: indicator J4 (m/s).

Models	Q1 (25%)	Median Line	Gap—Median	Q3 (75%)	Maximum
NSY240	51.799	53.825	0.00	56.556	63.699
HS250	51.495	53.267	0.558	55.640	61.898
NSY220	51.305	52.812	1.013	54.851	60.039
SY220	51.106	52.361	1.464	54.277	58.998
SY250	50.980	52.191	1.624	53.925	58.299

Figure 9 illustrates the consecutive times achieved by these models over short straight lines. A slight upward trend is observed from left to right, which is consistent with the observed speeds. Although the NSY240 model achieves notable speeds, its median times are inferior. Complementing this, Table 18 highlights the differences in sector 1 (S1). Notably, the first quartile times (Q1) are all above 0.5 s except for the NSY220 model. Simultaneously, the median times exceed one second for straight trajectories. The hybrid model shows a drop in performance relative to the SY250 model, which significantly improves its performance on straight lines. The behaviour of non-symmetrical models stands out, which is characterised by wheelbases between 220 mm and 240 mm and angular distances between 85 and 90 degrees. These models have an average weight of 318 g without a battery.

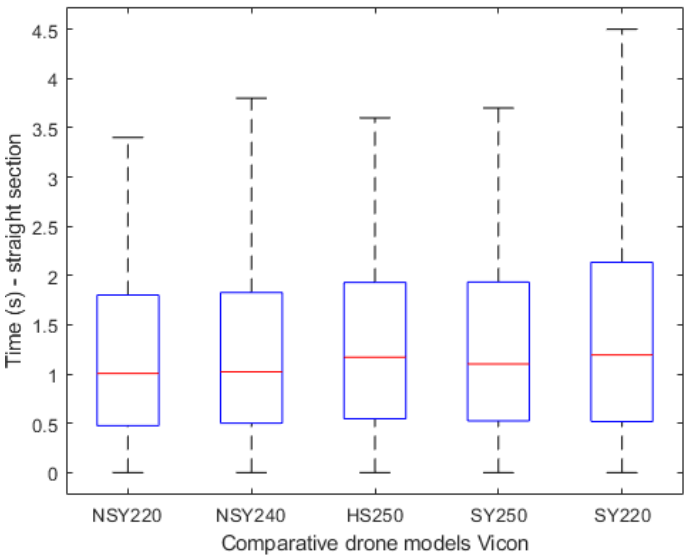

Figure 9. Straight time indicator.

Table 18. Straight time indicator (s).

Models	Q1 (25%)	Median Line	Gap—Median	Q3 (75%)	Maximum
NSY220	0.476	1.007	0.00	1.802	3.400
NSY240	0.502	1.023	0.016	1.827	3.800
SY250	0.524	1.103	0.096	1.933	3.700
HS250	0.547	1.117	0.110	1.930	3.599
SY220	0.518	1.194	0.187	2.134	4.500

It is evident that reducing the wheelbase (λ) tends to dominate control in this track sector. However, the angular distances (α, β) must be maintained. This reduction in wheelbase shortens the length between the propeller tips, resulting in a more compact racing drone. Consequently, the usefulness of arm length decreases in turning sectors.

4.3. Flight Sector 2 (S2)—Indicator: Tight Turn Trajectories (J5)

The behaviour of the models during tight turns is presented in this sector. The turning speeds and the time taken to traverse the track's S2 sector will be examined. As before, two diagrams of numerical quantities will be analysed, which are supported by two tables to complement the graphs. Additionally, the speeds of the models are illustrated in Figure 10.

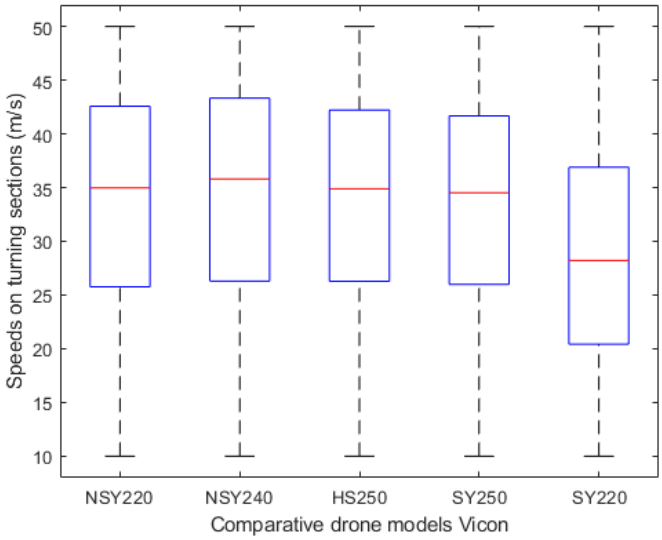

Figure 10. Performance indicator J5.

Firstly, a symmetrical data distribution is observed for all models, indicating a high similarity in the associated magnitudes. Secondly, a slight downward trend from left to right is evident, showing that the symmetric models achieve the lowest speeds overall. Notably, the SY250 model adheres to the median speed lines, whereas the NSY240 model stands out with the highest average speeds.

The indicative times for sector 2 (S2) are presented in Figure 11. The disparity in turning speed behaviour is evident with the SY220 model recording the highest times, reflecting poor turning performance. Additionally, the SY250 model aligns with the norm for times, while the hybrid model demonstrates a decline in performance. This result is inconsistent with its turning speed behaviour, as it achieves the lowest times but fails to demonstrate effective turn management.

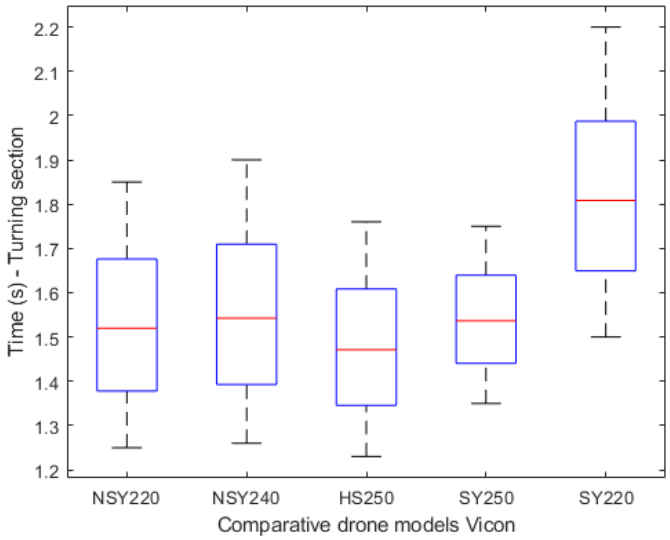

Figure 11. Turning time indicator.

Table 19 scales the magnitudes of the speeds, specifically highlighting the performance geometric attributes of the hybrid model. The HS250 hybrid model achieves one of the highest low speeds (Q1), reflecting its ability to accelerate quickly. However, it struggles to maintain consistent performance along turning trajectories, as indicated by its average speed (middle line). This behaviour aligns with its design philosophy, prioritising a balance between shape versatility and overall performance rather than specialising in geometric design.

Table 19. Speed turning behavior: indicator J5 (m/s).

Models	Q1 (25%)	Median Line	Gap—Median	Q3 (75%)
NSY240	26.303	35.806	0.00	43.320
NSY220	25.758	34.969	0.837	42.577
HS250	26.279	34.885	0.921	42.212
SY250	25.993	34.526	1.280	41.671
SY220	20.425	28.220	7.586	36.887

It is important to note that the acceleration experienced during turning trajectories is not caused by speed changes but rather by the abrupt changes in direction induced by the geometric features of the airframe. In contrast, the non-symmetrical NSY240 model achieves the highest low speeds (Q1) and intense medium speeds. Its design incorporates elongated arm lengths to fine-tune speed during turns, demonstrating exceptional turn-in consistency.

Although the hybrid and non-symmetrical models follow distinct performance patterns, both remain faithful to their respective design philosophies. The hybrid model, in particular, provides superior handling, as its design philosophy does not initially prioritise fast turns. Instead, the hybrid model aims for balanced behaviour through its geometric shape.

Table 20 presents the time management of the turning sector (S2) by quartiles. Notably, the gap between the intermediate models is reduced, providing a symmetrical distribution of these data. In contrast, the HS250 and SY220 models exhibit opposing behaviours. The hybrid model demonstrates uncommon turn control, while the symmetric model aligns with its known poor performance in fast turns. The results for this sector highlight the significance of the lambda length (λ). Initially, it is evident that the hybrid model benefits from this geometric attribute, featuring a wheelbase of 250 mm and an angular distance between 80 and 90 degrees. Its average weight is 323 g without a battery. However, its poor control over turning trajectories fails to translate its times into practical advantages. Additionally, the NSY240 model exhibits weak turning behaviour. Despite achieving the highest speeds, it records the longest times as it struggles to maintain an ideal trajectory.

Table 20. Turning time indicator (s).

Models	Q1 (25%)	Median Line	Gap—Median	Q3 (75%)
HS250	1.345	1.471	0.00	1.608
NSY220	1.377	1.519	0.048	1.676
SY250	1.440	1.536	0.065	1.639
NSY240	1.392	1.542	0.071	1.709
SY220	1.649	1.808	0.337	1.987

4.4. Performance Indicator for Accelerations (J6)

This section examines the accelerations of the racing drones. Two diagrams are presented to analyse the behaviour of this force: the first corresponds to the S1 sector, and the second to the turns in S2. Additionally, two tables linked to the quartiles of the recorded magnitudes are included. For comparison, the accelerations captured by the IMU are also

presented. Moreover, two sector diagrams, S1 and S2, are juxtaposed with the OMS-Vicon data as a validation tool.

Figure 12 illustrates the accelerations in the straight sector (S1). The behaviour of the data exhibits a lateral trend, indicating a high degree of similarity. Notably, the values around the median line are approximately 150 m/s^2, which are equivalent to around 15 gravities (g). However, the HS250 and SY250 models slightly exceed this trend. The data are concentrated near the lower quartile, as the maximum accelerations deviate significantly from the midline. Consequently, minimum accelerations occur more frequently.

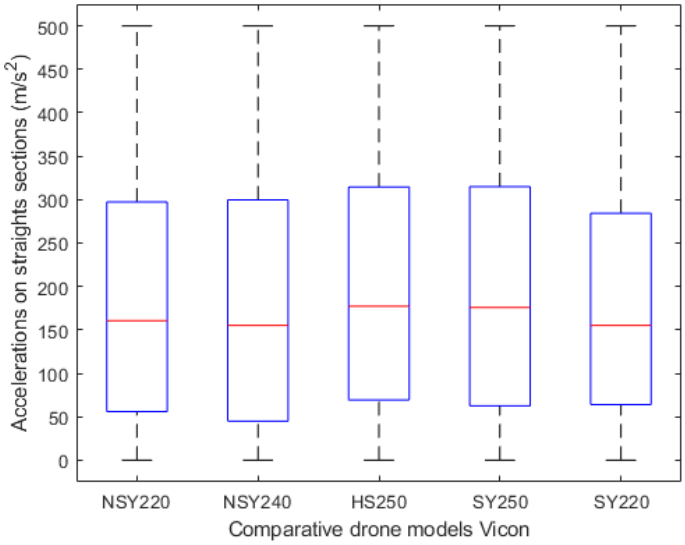

Figure 12. Performance indicator J6. Straight sector (S1).

In contrast, Figure 13 depicts the accelerations in sector 2 (S2) of the track, where an upward trend is observed as the wheelbase (λ) increases. The average acceleration in this sector is approximately 60 gravities (g). The stark difference compared to the straight sector is striking. This disparity is not due to the rated speeds in the two sectors (S1 and S2) but rather to the abrupt changes in the direction vector. It is also noteworthy that the hybrid models demonstrate exceptional acceleration. Unlike in the straight sector, they effectively manage to turn trajectories, which explains their consistent performance in both speed and time.

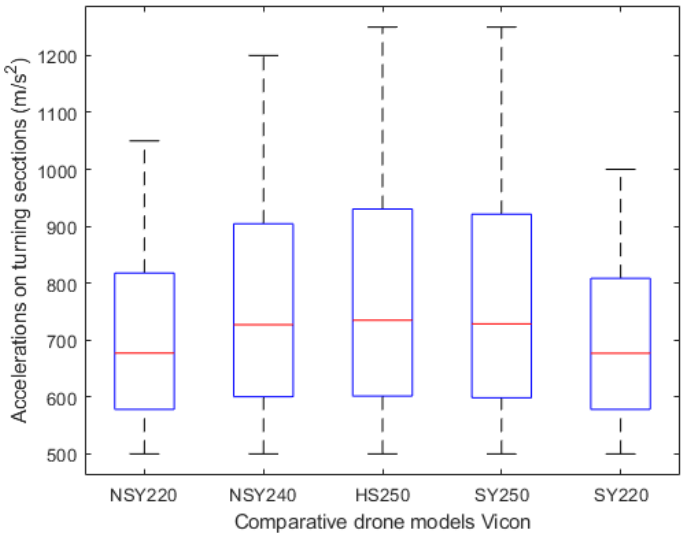

Figure 13. Performance indicator J6. Turning sector (S2).

It is also noteworthy that models with a wheelbase (λ) of 220.0 mm achieve similar acceleration but exhibit contrasting behaviours. The NSY220 model benefits from its geometric design, allowing it to handle trajectories effectively. In contrast, the SY220 model demonstrates the poorest performance indicators in both sectors.

Table 21 presents the acceleration trend. Firstly, the gap between the non-250 mm models exceeds 20.0 m/s^2, which is equivalent to approximately 18 gravities (g). Moreover, the data distribution indicates that this gap primarily arises in quartile 1 (Q1) with accelerations ranging from approximately 4.5 to 7.0 gravities (g). The behaviour of the NSY240 model is also noteworthy. The data spread is relatively small, resulting in the lowest accelerations among all models. Nevertheless, its speeds are consistent, and its straight-line times are well managed, suggesting that its trajectories closely approximate the ideal. The hybrid model achieves the highest accelerations, which explains its notable speeds on short straights. However, its times are among the highest, indicating trajectories that deviate from the race target.

Table 21. Acceleration straight behavior: indicator J6 (m/s^2).

Models	Q1 (25%)	Median Line	Gap—Median	Q3 (75%)
HS250	69.337	177.245	0.00	314.453
SY250	62.500	175.781	1.464	314.941
NSY220	55.909	160.644	16.601	297.363
SY220	63.965	155.280	21.965	284.179
NSY240	44.923	155.274	21.971	299.804

Table 22 presents the accelerations by quartiles. The behaviour of the SY250 model is particularly noteworthy. It exhibits lower accelerations toward Q1 compared to the HS250 and NSY240 models. However, its median line closely approaches the gap, effectively managing accelerations in tight turns. This aligns with its observed behaviour in terms of speeds and times in sector S2. Additionally, the maximum accelerations of these models range from 59 to 127 gravities (g). This highlights their suitability for sectors with turns and underscores the well-regarded geometric designs of these models.

Table 22. Acceleration turning behavior: indicator J6 (m/s^2).

Models	Q1 (25%)	Median Line	Gap—Median	Q3 (75%)	Maximum
HS250	601.562	734.864	0.00	930.175	1,250,000.0
SY250	598.633	728.516	6.348	921.386	1,250,000.0
NSY240	600.586	727.052	7.812	904.532	1,199,952.0
NSY220	578.126	677.246	57.618	817.872	1,049,926.0
SY220	578.126	676.757	58.107	808.595	1,000,000.0

4.5. Quality of Indicators—Comparative for Accelerations—IMU Vs VICON

This section presents the accelerations recorded by the inertial system, which have been organised to serve as authoritative data or benchmarks. In this way, a standard of reliability and accuracy is established. A comparison will be made between the readings from the two sensors, which are divided into two graphs: the first corresponding to the data from sector S1 and the second to sector S2. Additionally, Tables 23 and 24 are used to compute the percentage distribution of the data. Thus, the arithmetic difference between the two systems and the quality measure are provided.

Figure 14 comprises ten boxes, one for each model studied, comparing accelerations in sector one (S1). The first five boxes represent the IMU data, while the next five correspond to the OMS-Vicon data. The distribution of the IMU data is notably symmetrical, indicating that its average accelerations are relatively reliable. Firstly, it is observed that the IMU mean lines are above those of the OMS-Vicon. Secondly, the OMS-Vicon accelerations exhibit a

slight downward trend toward quartile 1 (Q1), suggesting that accelerations between 50.0% and 75.0% are less likely to be achieved.

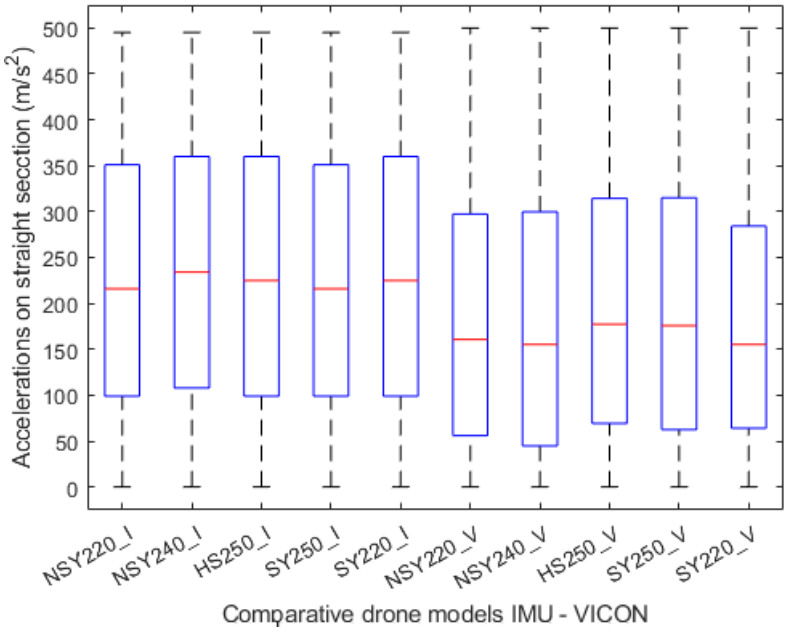

Figure 14. Comparative: straight sector acceleration (S1).

Table 23 provides a relative measure of the reliability of the data. Initially, the values grouped by the median line of the accelerations in S1 are described. Additionally, the arithmetic difference between the IMU and OMS-Vicon values is calculated. This method divides the reliability criteria into five levels: low, medium, medium high, high, and very high. Low reliability corresponds to accuracy values below 60%, while medium reliability covers the range of 60.0% to 70.0%. Medium high includes values between 70.0% and 80.0%, high reliability ranges from 80.0% to 90.0%, and very high exceeds 90%. This classification evaluates the reliability values of each model. For instance, the SY250 performance indicators (J) achieve high reliability for data linked to the S1 flight sector. In the annexes section, additional reliability values by quartiles are provided in Tables A1–A5.

Table 23. Data accuracy: median straight acceleration.

Median (50%)	SY250	NSY220	HS250	SY220	NSY240
IMU (m/s^2)	216.000	216.000	255.000	225.000	234.000
Difference (m/s^2)	40.219	55.356	77.755	69.720	78.726
Accuracy (%)	81.380	74.372	69.507	69.013	66.356
Reliability	High	Medium-H	Medium	Medium	Medium

Figure 15 illustrates the accelerations at the turns recorded by the two measurement systems. In the first case, the data follow a similar pattern, though not in magnitude, indicating a potential error action. This similarity confirms the reliability of the data values. In the second case, the OMS-Vicon system exhibits a slight downward trend with top accelerations less frequently achieved. Nevertheless, the similarity in patterns ensures consistent and trustworthy behaviour.

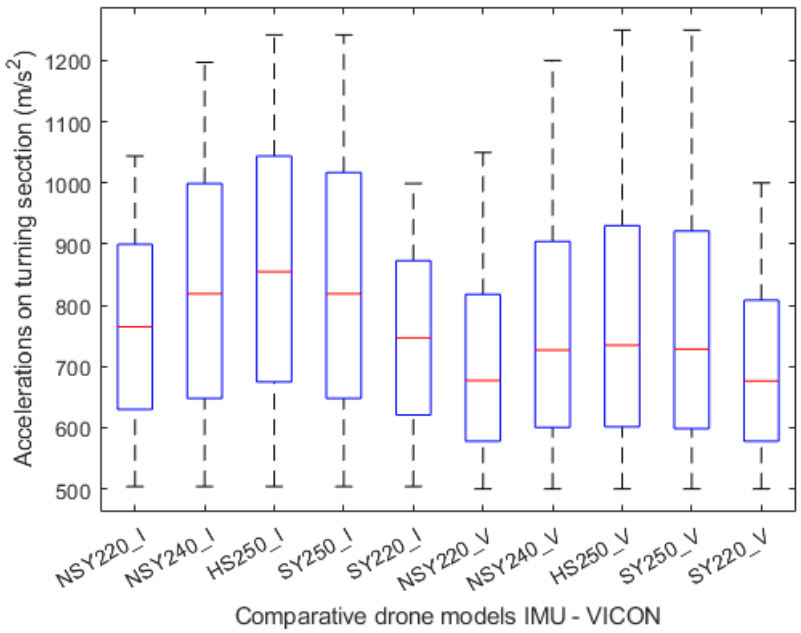

Figure 15. Comparative. Turning sector acceleration (S2).

Table 24 presents the reliability levels of flight in sector 2 (S2) and the corresponding accuracy percentages. Notably, the SY220 model stands out in both measures. The reliability of the other models generally ranges from medium to high with accuracy rates between 80.0% and 90.0%. However, the HS250 model exhibits the lowest values among all.

Table 24. Data accuracy: median turning acceleration.

Median (50%)	SY220	SY250	NSY240	NSY220	HS250
Q1/IMU (m/s^2)	747.000	819.000	819.000	765.000	855.000
Difference (m/s^2)	70.243	90.484	91.948	87.754	120.136
Accuracy (%)	90.596	88.951	88.773	88.528	85.949
Reliability (%)	V-High	Medium-H	Medium-H	Medium-H	Medium-H

4.6. Results Update

In the previous study, the behaviour of racing drones was defined. Firstly, a racing track with long sectors and wide turns was considered. Secondly, a Doppler sensor system was used to capture the motion. The current study provides an update. A track with shorter sectors in confined spaces and a technical database for training autonomous racing drones has been used. The results are summarised as follows: hybrid and symmetrical models demonstrate exceptional acceleration. Long wheelbases (λ) enhance the pitching moment, improving horizontal motion. Similarly, large angular distances (α) enhance the turning moment. Consequently, the hybrid model tends to create a gap during tight turns. However, its control over short straight and short turning trajectories is poor, meaning these geometric advantages do not translate into optimal lap times. Non-symmetric models also exhibit poor acceleration in confined spaces. Nevertheless, they handle trajectories efficiently. Their elongated shape improves turning ability, resulting in the best lap times. It should be noted that an increased wheelbase (λ) reduces responsiveness. Therefore, the design compromise lies within a 30 mm range.

Table 25 presents the accuracy of indicator J4. Overall, the results are generally consistent with a medium scale, indicating that the indicator's forecast achieves an accuracy of up to 70%. Notably, the symmetrical structures exhibit a highly accurate indicator, exceeding 70.0%. However, they are not the most efficient, representing a geometric

turning point in the design process. Non-symmetric structures suggest more efficient control in this sector with an indicator accuracy of up to 80.0%. This level of accuracy on a medium-high scale signifies a positive design midpoint. For instance, it is suitable for training an autonomous drone.

Table 25. Short straight line (J4): sector (S1)—16 metres.

Model	λ (mm)	(α, β) Angular Distances	Speed (m/s)	Acc (m/s^2)	Time (s)	Data Accuracy
NSY	220.0	$70.0^\circ \leq (\alpha, \beta) \leq 90.0^\circ$	52.812	160.644 (16.5 g)	1.007	Medium-H
NSY	240.0	$80.0^\circ \leq (\alpha, \beta) \leq 90.0^\circ$	53.825	155.274 (16.0 g)	1.023	Medium
SY	250.0	$(\alpha, \beta) \equiv 90.0^\circ$	52.191	175.781 (18.0 g)	1.103	High
HS	250.0	$\alpha \equiv 80.0^\circ, \beta \neq 90.0^\circ$	53.267	177.245 (18.0 g)	1.117	Medium
SY	220.0	$(\alpha, \beta) \equiv 90.0^\circ$	52.361	155.280 (16.0 g)	1.194	Medium

Table 26 presents the reliability of the J5 indicator for each model. These data fall within an accuracy range exceeding 70.0%, indicating that the indicator for tight turns is representative. Notably, the symmetrical model with a wheelbase of 220.0 mm demonstrates highly accurate data, meaning its behaviour is faithfully represented. However, its control over tight turns is poor. The symmetrical model's characteristics provide an excellent starting point for aerodynamic design. However, when the objective is to train a racing drone to complete an autonomous trajectory for competition, the hybrid model emerges as the most suitable choice for this sector.

Table 26. Tight turn (J5): sector (S2)—2.5 metres.

Model	λ (mm)	(α, β) Angular Distances	Speed (m/s)	Acc (m/s^2)	Time (s)	Data Accuracy
HS	250.0	$\alpha \equiv 80.0^\circ, \beta \neq 90.0^\circ$	34.885	734.864 (75 g)	1.471	Medium-H
NSY	220.0	$70.0^\circ \leq (\alpha, \beta) \leq 90.0^\circ$	34.969	677.246 (69 g)	1.519	Medium-H
SY	250.0	$(\alpha, \beta) \equiv 90.0^\circ$	34.526	728.516 (74 g)	1.536	Medium-H
NSY	240.0	$80.0^\circ \leq (\alpha, \beta) \leq 90.0^\circ$	35.806	727.052 (74 g)	1.542	Medium-H
SY	220.0	$(\alpha, \beta) \equiv 90.0^\circ$	28.220	676.757 (69 g)	1.808	V-High

In prior work [1], the pilots argued that symmetric structures are smoothly manoeuvrable, while non-symmetric structures were described as agile and well suited for tight turns. However, earlier tests revealed a notable contradiction: symmetric structures performed better on wide tracks and lengthy sectors. Despite this, pilots consistently preferred non-symmetrical designs. The new findings clarify this dichotomy. The updated track is more confined with shorter straight lines than the previous one. These conditions result in more frequent turns compared to larger tracks. Considering the design of the new track, the indicators demonstrate that non-symmetrical structures outperform symmetrical ones across all sectors. The key feature of non-symmetrical structures is their elongated shape, which provides a distinct advantage in rolling. Consequently, non-symmetric structures respond more rapidly to constant changes in trajectory.

5. General Conclusions

This study continues to advance the understanding of the dynamics of racing drones. In this iteration, the motion dynamics are addressed through extensive data analysis. The data were labelled using the J4, J5, and J6 performance indicators, representing speed (J4), time (J5), and acceleration (J6). The results demonstrated a significant increase in trustworthiness attributed to using an optical sensor system for data collection. In contrast, the previous study primarily relied on Doppler sensors, although it utilised a considerably larger racetrack.

The robust analysis of the results highlights the qualities of the optical motion system (OMS) and the experimental design in characterising the dynamic behaviour of racing

drones on confined tracks. These findings underscore the OMS's data storage capabilities, yielding highly accurate and consistent data supported by the TRAM FPV database. The findings reveal significant variations in performance based on geometric layouts: symmetric drones (SY) demonstrate stability and regulation on straight trajectories. With their elongated designs, non-symmetric drones (NSY) effectively utilise manoeuvrability in tight curves. Hybrid drones (HS) balance stability and adaptability, delivering a trade-off—the moderate performance in straight sectors is offset by the excellent performance in curved sectors. A pivotal insight is the connection between acceleration during turning and sharp directional changes driven by geometric features rather than the usual physical shifts at the transition between curves and straight lines. This observation aligns with previous studies and reinforces the robustness of the findings even under more restrictive flight conditions and experimental tests. Furthermore, the robust design and extensive volume of TRAM FPV data mitigate potential errors and ensure precise insights for complex navigation environments. As such, the flight analysis outputs position this data-driven approach as a reliable tool for advancing research in drone dynamics. Its potential extends beyond racing-quality drones, enabling the development of new and optimised concepts in dynamic drone design.

The reliability of the data was evaluated using acceleration data (IMU vs. OMS) linked to airframe shapes based on their performance across different trajectories. Symmetric shapes are easily managed on various types of racetracks. Additionally, non-symmetric designs offer a time advantage on hindered flight trajectories. For cross-flight trajectories, hybrid models emerge as a suitable choice. These are effective for sectors with long and obstructed trajectories and well suited for wide and sharp curves. However, both non-symmetric and hybrid designs require careful adjustments in terms of control aids. Non-symmetric models must be precisely tuned to perform strongly on long sectors, requiring adjustments for long and tight turns. Similarly, hybrid shapes demand appropriate control settings to optimise performance. With these adjustments, these airframes can achieve high racing performance indicators.

The new results highlight a significant disparity in the behaviour of racing drones on long and smaller racetracks. Symmetric airframes excel on long and wide racetracks due to their high manoeuvrability and stability. In contrast, non-symmetrical structures perform better on short tracks and tight turns. Studies indicate that elongated geometries respond more effectively to frequent trajectory shifts. Hybrid structures offer an intermediate solution to the challenges posed by varying track lengths. However, they must be designed with large angular distances and extended wheelbases to gain a competitive edge in racing. Additionally, the reliability of the data supports mathematical modelling for detached trajectories of a race track. The accuracy of the data enables model parameters to be refined using test data, facilitating the design of tailored controllers for specific trajectories.

The current statistical analysis utilises data collected on an oval track layout with an operational width limited to 5 m. This controlled environment effectively validates the proposed methodologies. Expanding the analysis to more complex tracks with multiple obstacles and variable altitudes could provide additional insights into the system's software adaptability and robustness, extending beyond the current dynamic analysis. However, conducting statistical analysis on such intricate track layouts would significantly reduce the availability of laboratories capable of housing large-scale facilities. For this reason, the tailored TRAM FPV database has been employed. It provides a sufficiently robust volume of data to support the analysis. Moreover, the laboratory layout where it was developed aligns optimally with the manufacturers' specifications.

In practical terms, the Optical Motion Capture System (OMS), renowned for its high measurement accuracy and real-time data processing capabilities, requires a minimum of two cameras to track drones with the desired level of precision effectively. The ideal factory setup recommends controlled tracks measuring $10 \times 10 \times 5$ m and uniform lighting conditions, as demonstrated in the flight arena laboratories at Cranfield University. Notably, the flight arena is one of the largest indoor facilities of its kind, ranking as the second largest

worldwide. Additionally, high-difficulty scenarios test the ability of the Vicon Tracker software to maintain accurate tracking. In applications beyond those covered in this study, such as machine learning, the lack of precision can be mitigated by incorporating more data labels and extending training hours to enrich the dataset. This analytical methodology leverages the ability to capture high-speed dynamic manoeuvres with accuracy, making it highly suitable for the type of analysis conducted in this study. Future work in this line of statistical analysis will focus on exploring more complex scenarios. The emphasis will be on integrating OMS data with advanced algorithms from other sensor sources rather than increasing the complexity of the physical layout.

The findings of this study underscore the robustness of the TRAM FPV database, which was meticulously developed within the laboratories at Cranfield University. This resource is particularly notable for its capability to capture and analyse the dynamic behaviour of racing drones under controlled conditions. A crucial consideration is the potential applicability of this framework to other types of drones, particularly those with varying sizes, weights, and propulsion systems. The adaptability of OMS systems to mixed designs is largely attributed to their high-precision tracking capabilities and flexible calibration processes within controlled environments. This versatility extends the applicability of such sensors across a wide range of drone designs and enhances the overall utility and reliability of the database. The analysis conducted in this study leverages the inherent design of the TRAM FPV database, further reinforcing the soundness of the results. However, factors such as the alignment of reflective markers, the airframe geometry of the drone, and flight speed can significantly influence tracking accuracy and data quality. Moreover, maintaining appropriate distances between markers and ensuring an adequate number of markers are critical to avoiding measurement inconsistencies and mitigating reflections caused by other fluorescent-coloured sources. These considerations must also consider the physical limitations of the flight arena, including its size boundaries and the cameras' field of view.

The dataset utilised in this study focuses on lightweight racing drones with a weight limit of up to 500 g and a wheelbase of approximately 500 mm. Consequently, the systematic methodology and statistical approach developed here are robust and well suited for motion analysis, physics-informed modelling, and dynamic studies within this operational range. Larger drones, such as those employed in cargo delivery or surveillance applications, could also benefit from the OMS system's accuracy and the conceptual framework of this database, provided that the experimental setting is scaled to accommodate their size and operational requirements. However, scaling the system introduces additional challenges and risks. For example, larger drones or those utilising non-electric propulsion systems, such as internal combustion engines, may generate higher levels of vibration and noise, potentially affecting the precision of OMS tracking and the reliability of collected data. These systems also require larger operational volumes, which complicates the calibration and optimisation of the control volume. Furthermore, the current infrastructure can only support such analyses by incorporating GNSS systems, enabling accurate tracking over extended areas.

Finally, safety considerations are paramount when scaling up to larger drones. Increased mass and alternative propulsion systems result in higher kinetic energy, posing greater risks during testing. Ensuring robust safety protocols and implementing risk mitigation measures is essential to safely expand the applicability of the OMS system and database. Despite these challenges, the OMS system retains the theoretical capability to track other types of vehicles by optimising marker placement, calibrating the control volume, and adapting storage configurations. This methodology's versatility thus offers promising potential for broader applications albeit with the necessity of addressing the associated risks. A core strength of this study is the robustness of the TRAM FPV database, which is supported by the substantial volume of data stored, processed, and analysed as an integrated unit. The extensive dataset, structured and refined across various flight tests, significantly reduces potential issues such as camera occlusions. Indeed, data jumps or discontinuities that might occur during high-speed manoeuvres are effectively mitigated. Furthermore, the

database design accounts for relative measurement errors introduced during calibration. These features ensure the high reliability and consistency of the collected data.

The Vicon system, whilst highly accurate, operates within a fixed control volume. This controlled space depends on the number and placement of cameras. In the flight arena, the control volume typically spans 10 × 10 × 5 m, ensuring coverage of the full range of drone trajectories within this confined space. However, reflective markers occasionally shift outside the proper view of individual cameras during fast manoeuvres. This physical limitation can result in transient tracking errors or marker loss. Rapid changes in marker visibility may also introduce sampling errors or increase noise in the recorded data. Additionally, wall vibrations caused by airflow wakes during high-speed rotations can affect measurement accuracy. Despite these practical challenges, the high-density dataset provided by the TRAM FPV database enables robust statistical filtering and error proofing during data processing. This fault tolerance ensures that the analysed information remains consistent and accurate. The flight arena's white lighting system comprises 43 panels measuring 123 × 62 centimetres. This system spans the control volume and minimises the impact of variable light intensity. Moreover, the lighting intensity is adjustable, enhancing marker visibility and tracking performance. By maintaining uniform lighting conditions, the flight arena ensures reliable camera operation. These features reduce the likelihood of data loss or mismatches during high-speed testing and support reliable data storage.

The factors discussed have significantly contributed to the robustness and versatility of the TRAM FPV database. The data quality establishes the database as a highly reliable resource for studying the dynamic behaviour of drones. Despite the inherent challenges of high-speed dynamic tracking and the physical constraints of the control volume, the database's comprehensive design and extensive data volume provide a solid foundation for rigorous studies requiring high precision and repeatability. This approach ensures a quantifiable margin of error, making the statistical insights practically applicable. Moreover, the demonstrated reliability of all tools and resources is intended to support both current and future applications even under suboptimal conditions.

Author Contributions: Conceptualization, J.M.C.Q. and S.G.-N.; Methodology, S.G.-N. and J.M.C.Q.; Software, J.M.C.Q. and S.G.-N.; Validation, J.M.C.Q., S.G.-N., R.S. and D.I.I.; Formal analysis, S.G.-N.; Investigation, J.M.C.Q., S.G.-N., R.S. and D.I.I.; Writing—original draft, J.M.C.Q.; Writing—review and editing, S.G.-N., R.S. and D.I.I.; Supervision, D.I.I. and S.G.-N.; Project administration, S.G.-N.; Funding acquisition, S.G.-N. All authors have read and agreed to the published version of the manuscript.

Funding: This work has been supported by the Spain government via MCIN/AEI/ 10.13039/501100011033 [Project PID2020-119468RA-I00].

Data Availability Statement: The data presented in this study are available in this paper and the repository: https://dspace.lib.cranfield.ac.uk/handle/1826/18343 (accessed on 29 October 2024).

Conflicts of Interest: The authors declare no conflicts of interest.

Appendix A

Table A1. Data accuracy: Q1 straight acceleration.

Q1 (25%)	HS250	SY220	SY250	NSY220	NSY240
IMU (m/s^2)	99.001	99.001	99.001	99.001	108.005
Difference (m/s^2)	29.664	35.036	36.501	43.092	63.082
Accuracy (%)	70.036	64.610	63.130	56.473	41.593
Reliability	Medium-H	Medium	Medium	Low	Low

Table A2. Data accuracy: Q3 straight acceleration.

Q3 (75%)	SY250	HS250	NSY220	NSY240	SY220
IMU (m/s^2)	351.000	360.000	351.000	360.000	360.000
Difference (m/s^2)	36.059	45.547	53.637	60.196	75.821
Accuracy (%)	89.726	87.348	84.718	83.278	78.938
Reliability	High	High	High	High	Medium-H

Table A3. Data accuracy: Q1 turning acceleration.

Q1 (25%)	SY220	NSY240	SY250	NSY220	HS250
IMU (m/s^2)	621.000	648.000	648.000	630.000	675.000
Difference (m/s^2)	42.874	47.414	49.367	51.874	73.438
Accuracy (%)	93.095	92.683	92.381	91.766	89.120
Reliability	V-High	V-High	V-High	V-High	High

Table A4. Data accuracy: Q3 turning acceleration.

Q3 (50%)	SY220	NSY220	SY250	NSY240	HS250
IMU (m/s^2)	873.000	900.000	1017.0	999.000	1044.0
Difference (m/s^2)	64.405	82.128	95.614	94.468	113.825
Accuracy (%)	92.622	90.874	90.598	90.543	89.097
Reliability	V-High	V-High	V-High	V-High	Medium-H

Table A5. Data accuracy: maximum turning acceleration.

Maximum	SY250	HS250	SY220	NSY220	NSY240
IMU (m/s^2)	1242.000	1242.000	999.000	1044.000	1197.000
Difference (m/s^2)	−8.00	−8.00	−1.00	−5.926	−2.952
Accuracy (%)	100.0	100.0	100.0	100.0	100.0
Reliability	V-High	V-High	V-High	V-High	V-High

References

1. Castiblanco, J.M.; Garcia-Nieto, S.; Simarro, R.; Salcedo, J. Experimental study on the dynamic behaviour of drones designed for racing competitions. *Int. J. Micro Air Veh.* **2021**, *13*, 17568293211005757. [CrossRef]
2. Costa, G.; Pinho, J.; Botto, M.A.; Lima, P.U. Online learning of MPC for autonomous racing. *Robot. Auton. Syst.* **2023**, *167*, 104469. [CrossRef]
3. Song, Y.; Steinweg, M.; Kaufmann, E.; Scaramuzza, D. Autonomous drone racing with deep reinforcement learning. In Proceedings of the 2021 IEEE/RSJ International Conference on Intelligent Robots and Systems (IROS), Prague, Czech Republic, 27 September–1 October 2021; pp. 1205–1212.
4. De Wagter, C.; Paredes-Vallés, F.; Sheth, N.; De Croon, G. Learning fast in autonomous drone racing. *Nat. Mach. Intell.* **2021**, *3*, 923–923. [CrossRef]
5. Castiblanco Quintero, J.; Garcia-Nieto, S.; Ignatyev, D.; Blasco, X. The TRAM-FPV RACING Open Database. Sequences complete indoor flight sequences for the stuty of racing drones. In Proceedings of the XLIII Jornadas de Automática, Universidade da Coruña. Servizo de Publicacións, La Rioja, Spain, 7–9 September 2022; pp. 341–352.
6. Castiblanco Quintero, J.; Garcia-Nieto, S.; Simarro, R.; Salcedo, J. Co-simulation platform for geometric design, trajectory control and guidance of racing drones. *Int. J. Micro Air Veh.* **2022**, *14*, 17568293221143785. [CrossRef]
7. Vicon Motion Systems Ltd. *Vicon Tracker User Guide*; Revision 2, for use with Tracker 4.1; Vicon Motion Systems Ltd.: Oxford, UK, 2024.
8. Vicon Motion Systems Ltd. Vicon Tracker. 2024. Available online: https://help.vicon.com/download/attachments/14320520/Vicon%20Tracker%20User%20Guide.pdf (accessed on 21 November 2024).

9. Moon, H.; Martinez-Carranza, J.; Cieslewski, T.; Faessler, M.; Falanga, D.; Simovic, A.; Scaramuzza, D.; Li, S.; Ozo, M.; De Wagter, C.; et al. Challenges and implemented technologies used in autonomous drone racing. *Intell. Serv. Robot.* **2019**, *12*, 137–148. [CrossRef]
10. Katsampiris-Salgado, K.; Haninger, K.; Gkrizis, C.; Dimitropoulos, N.; Krüger, J.; Michalos, G.; Makris, S. Collision detection for collaborative assembly operations on high-payload robots. *Robot. Comput.-Integr. Manuf.* **2024**, *87*, 102708. [CrossRef]
11. Pavliv, M.; Schiano, F.; Reardon, C.; Floreano, D.; Loianno, G. Tracking and relative localization of drone swarms with a vision-based headset. *IEEE Robot. Autom. Lett.* **2021**, *6*, 1455–1462. [CrossRef]
12. Edriss, S.; Romagnoli, C.; Caprioli, L.; Zanela, A.; Panichi, E.; Campoli, F.; Padua, E.; Annino, G.; Bonaiuto, V. The Role of Emergent Technologies in the Dynamic and Kinematic Assessment of Human Movement in Sport and Clinical Applications. *Appl. Sci.* **2024**, *14*, 1012. [CrossRef]
13. Li, Y.; Scanavino, M.; Capello, E.; Dabbene, F.; Guglieri, G.; Vilardi, A. A novel distributed architecture for UAV indoor navigation. *Transp. Res. Procedia* **2018**, *35*, 13–22. [CrossRef]
14. Li, S.; De Wagter, C.; de Visser, C.; Chu, Q.; de Croon, G. In-flight model parameter and state estimation using gradient descent for high-speed flight. *Int. J. Micro Air Veh.* **2019**, *11*, 1756829319833685. [CrossRef]
15. Hamdi, A.; Salim, F.; Kim, D.Y. DroTrack: High-speed Drone-based Object Tracking Under Uncertainty. In Proceedings of the 2020 IEEE International Conference on Fuzzy Systems (FUZZ-IEEE), Glasgow, UK, 19–24 July 2020; pp. 1–8.
16. Li, S.; Ozo, M.M.; De Wagter, C.; de Croon, G.C. Autonomous drone race: A computationally efficient vision-based navigation and control strategy. *Robot. Auton. Syst.* **2020**, *133*, 103621. [CrossRef]
17. Du, H.; Wang, W.; Xu, C.; Xiao, R.; Sun, C. Real-time onboard 3D state estimation of an unmanned aerial vehicle in multi-environments using multi-sensor data fusion. *Sensors* **2020**, *20*, 919. [CrossRef] [PubMed]
18. Queralta, J.P.; Almansa, C.M.; Schiano, F.; Floreano, D.; Westerlund, T. Uwb-based system for uav localization in gnss-denied environments: Characterization and dataset. In Proceedings of the 2020 IEEE/RSJ International Conference on Intelligent Robots and Systems (IROS), Las Vegas, NV, USA, 25–29 October 2020; pp. 4521–4528.
19. Mashood, A.; Mohammed, M.; Abdulwahab, M.; Abdulwahab, S.; Noura, H. A hardware setup for formation flight of UAVs using motion tracking system. In Proceedings of the 2015 10th IEEE International Symposium on Mechatronics and Its Applications (ISMA), Sharjah, United Arab Emirates, 8–10 December 2015; pp. 1–6.
20. Furtado, J.S.; Liu, H.H.; Lai, G.; Lacheray, H.; Desouza-Coelho, J. Comparative analysis of optitrack motion capture systems. In *Advances in Motion Sensing and Control for Robotic Applications*; Springer: Berlin/Heidelberg, Germany, 2019; pp. 15–31.
21. Kaufmann, E.; Gehrig, M.; Foehn, P.; Ranftl, R.; Dosovitskiy, A.; Koltun, V.; Scaramuzza, D. Beauty and the beast: Optimal methods meet learning for drone racing. In Proceedings of the 2019 IEEE International Conference on Robotics and Automation (ICRA), Montreal, QC, Canada, 20–24 May 2019; pp. 690–696.
22. Jung, S.; Lee, H.; Hwang, S.; Shim, D.H. Real time embedded system framework for autonomous drone racing using deep learning techniques. In *2018 AIAA Information Systems-AIAA Infotech@ Aerospace*; AIAA: Washington, DC, USA, 2018; p. 2138.
23. Conconi, M.; Pompili, A.; Sancisi, N.; Parenti-Castelli, V. Quantification of the errors associated with marker occlusion in stereophotogrammetric systems and implications on gait analysis. *J. Biomech.* **2021**, *114*, 110162. [CrossRef] [PubMed]
24. Rahimian, P.; Kearney, J.K. Optimal camera placement for motion capture systems. *IEEE Trans. Vis. Comput. Graph.* **2016**, *23*, 1209–1221. [CrossRef] [PubMed]
25. Castiblanco, J.M.; Garcia-Nieto, S.; Ignatyev, D.; Blasco, X. THE TRAM-FPV RACING Open Database: Sequences Complete Indoor Flight Tests for the Study of RACING drones. 2024. Available online: https://dspace.lib.cranfield.ac.uk/handle/1826/18343 (accessed on 26 November 2024).
26. *ISO 10360-10:2021*; Geometrical Product Specifications (GPS)—Acceptance and Reverification Tests for Coordinate Measuring Systems (CMS)—Part 10: Laser Trackers for Measuring Point-to-Point Distances. International Organization for Standardization: Geneva, Switzerland, 2021.
27. *ISO 8995-1:2002*; Lighting of Work Places—Part 1: Indoor Work Places. International Organization for Standardization: Geneva, Switzerland, 2002.
28. *ISO 9241-303:2011*; Ergonomics of Human-System Interaction—Part 303: Requirements for Electronic Visual Displays. International Organization for Standardization: Geneva, Switzerland, 2011.
29. *ISO/IEC 17025:2017*; General Requirements for the Competence of Testing and Calibration Laboratories. International Organization for Standardization: Geneva, Switzerland, 2017.
30. *ISO 9001:2015*; Quality Management Systems—Requirements. International Organization for Standardization: Geneva, Switzerland, 2015.

Improving racing drones flight analysis: a data-driven approach using motion capture systems

Castiblanco Quintero, Jose M.

2024-12-09

Castiblanco Quintero JM, Garcia-Nieto S, Simarro R, Ignatyev DI. (2024) Improving racing drones flight analysis: a data-driven approach using motion capture systems. Drones, Volume 8, Issue 12, December 2024, Article number 742

https://doi.org/10.3390/drones8120742